Adsorption Study of Al^{3+}, Cr^{3+}, and Mn^{2+} onto Quartz and Corundum using Flow Microcalorimetry, Quartz Crystal Microbalance and Density Functional Theory

Nicholas Allen[†,1], Chong Dai[†,2], Yandi Hu[2], James D. Kubicki[3], and Nadine Kabengi[1, 4*]*

[1]Georgia State University, Department of Chemistry, Atlanta, GA 30303, USA

[2] University of Houston, Department of Civil and Environmental Engineering, Houston, TX 77004, USA

[3] University of Texas at El Paso, Department of Geological Sciences, El Paso, TX 79968, USA

[4]Georgia State University, Department of Geosciences, Atlanta, GA 30303, USA

[†] **Equal Contribution**

[*]Co-corresponding author emails: yhu11@uh.edu ; kabengi@gsu.edu;

Abstract

The adsorption of aqueous ions onto natural mineral surfaces controls numerous mineral-water interactions and is governed by, among other numerous factors, ion dehydration and hydrolysis. This work explored the extent to which dehydration and hydrolysis affect the adsorption of three metal cations, Al^{3+}, Cr^{3+}, and Mn^{2+}, onto quartz (SiO_2) and corundum (Al_2O_3) surfaces at pH 3.8 through the integration of flow microcalorimetry (FMC), quartz crystal microbalance with dissipation (QCM-D) measurements and density functional theory (DFT) calculations. At pH 3.8, negligible amounts of Mn^{2+} and Al^{3+} are hydrolyzed, while 78% of Cr^{3+} exist in hydrolyzed species. QCM-D and FMC measurements showed that Al^{3+} and Cr^{3+} adsorb to both surfaces, while Mn^{2+} adsorbed only to Al_2O_3. DFT bond energy calculations confirmed the favorable bonding between the mineral surfaces and Al^{3+} and Cr^{3+}, and that Mn^{2+} adsorption onto SiO_2 was unfavorable. Furthermore, FMC showed that on both surfaces, the adsorption of Al^{3+} was endothermic and reversible, while that of Cr^{3+} was exothermic and partially irreversible. Through the integration of experimental and computational methods, this work suggested that the reversible adsorption of unhydrolyzed cations (Mn^{2+} and Al^{3+}) occurred through weak electrostatic interactions. The large energy cost required to dehydrate unhydrolyzed cations resulted in an endothermic adsorption process. Meanwhile, hydrolyzed Cr^{3+} species can adsorb on quartz and corundum through covalent-bond formation and thus their adsorption was partially irreversible. Furthermore, the hydrolysis of Cr^{3+} lowered the dehydration energy during adsorption resulting in an exothermic adsorption. By using bond energies as a guide to indicate the possibility of thermodynamically favored adsorption, there was a strong agreement between the DFT and experimental techniques. The findings presented here contribute to understanding and predicting various mineral-water interfacial processes in natural environment.

Key words: flow microcalorimetry (FMC); quartz crystal microbalance with dissipation (QCM-D); density functional theory (DFT) calculations; endothermic and exothermic; reversibility; ion hydrolysis; ion dehydration; bond energy;

1. Introduction

The adsorption of aqueous ions onto natural mineral surfaces controls numerous mineral-water interactions.[1-7] Oxygen (O), Silicon (Si) and Aluminum (Al) are the three most abundant elements in Earth's crust, their bonds, (i.e. Si-O and Al-O, are thus the building blocks of a large number of crustal minerals, such as oxides, quartz, feldspars, clays, and micas.[8, 9] Of these minerals, both aluminum and silicon oxides are common components that play key roles in a number of interfacial processes, such as mineral precipitation and dissolution,[10-12] oxidation-reduction,[13, 14] and contaminant transport [15-18], all of which have far-reaching implications for biogeochemical processes[10-14]. Therefore, it is significant to better understand the underlying mechanisms governing ion adsorption and exchange onto mineral surfaces with Si-O and Al-O bonds exposed to solutions.

Quartz (SiO_2) is the primary crystalline structure of the silicon oxides family. Compared to other minerals and metal oxides, quartz possesses unique chemical properties, in particular, a low point-of-zero-charge (pHpzc) reported between pHs of 1.5 to 2.8 and a low dielectric constant (ε) of 4.3.[19-24] In the aluminum oxides, corundum is the most commonly occurring and the most thermodynamically stable crystalline polymorph.[25, 26] The pH_{pzc} of corundum has been reported to range between pHs 8.0−10.0 for powders and pHs 5.0−7.0 for specific crystal planes, and its dielectric constant (ε) is 10.4.[23, 27] These values are significantly different from those reported for quartz. Both minerals offer an opportunity to study potentially contrasting effects on underlying mechanisms and were thus chosen for this work. Quartz and corundum were chosen in this study to represent minerals with Si-O and Al-O bonds exposed to solutions for ion adsorption.

Previous studies have reported that metal ions adsorption onto minerals could be affected by their charge, hydrolysis and dehydration properties. To dissect the extent to which each of these

cation-specific properties controls adsorption, we have chosen to study Al^{3+}, Cr^{3+}, and Mn^{2+}, three cations that are not only abundant in the environment but also offer contrasting hydration and hydrolysis properties. Al^{3+} is the most abundant metal ion in natural environments and is phytotoxic. Mn^{2+} is the second most abundant transition metal and a key redox agent in soils. Cr^{3+} is a hazardous contaminant in many soils and aquifers. Although Al^{3+} is redox inactive, both Cr^{3+} and Mn^{2+} participate in geochemical redox processes. The hydrated radii of both Mn^{2+} and Al^{3+} are similar at 4.38 Å,[28] while that of Cr^{3+} is smaller at 4.75 Å).[28] The hydrolysis constants at 25 ˚C were reported as 4×10^{-15}, 7×10^{-31} and 2×10^{-13} for Al^{3+}, Cr^{3+}, and Mn^{2+}respectively.[29]

Studies of Al^{3+} adsorption onto mineral surfaces have included clays and silica.[30] Using batch adsorption methods, Bloom and McBride[31] found that at pH 4.0, Al^{3+} can be hydrolyzed to $AlOH^{2+}$ and adsorbed on smectite. Walker et al,[32] using a flow-through stirred-cell system, found no measurable hydrolysis during the adsorption of Al^{3+} onto clay minerals between pHs 3-4, and asserted the adsorption to be predominantly an electrostatic outer-sphere exchange. On the other hand, Kuan et al,[30] using a combination of batch adsorption and surface complexation modeling, determined Al^{3+} adsorption on silica to occur predominantly as inner-sphere interaction and that hydrolyzed Al^{3+} was the dominant form of absorbed species at pH of 3.0 and higher.

The adsorption of Cr^{3+} has been widely studied on δ-aluminum oxide,[33] ferrihydrite,[34] and silica.[35-37] Wehrli et al[33] determined that Cr^{3+} adsorbed on δ-aluminum oxide as the hydrolyzed species ($CrOH^{2+}$) and formed bidentate complexes at pHs of 2.5 - 6.0. On ferrihydrite, Charlet and Manceau[34] found Cr^{3+} interactions with the surface to occur as inner-sphere $CrOH^{2+}$complexes at low surface coverage, and as chromium oxy-hydroxide surface precipitation at high surface coverages. On silica, Fendorf et al.[35, 36] found that $CrOH^{2+}$ formed monodentate inner-sphere complexes at low coverage.

Studies of Mn^{2+} adsorption included those on iron oxides,[13, 38] aluminum oxides,[39] and silica.[40] On the δ-aluminum oxide and iron oxide surfaces, Davies and Morgan[13] determined that in basic solutions (pH > 7.5), Mn^{2+} forms both monodentate and bidentate complexes although hydrolysis was not considered during the adsorption process. Hachiya et al.[41] concurred with Bloom and McBride[31] in that they reported that divalent cations (e.g. Mn^{2+}) adsorbed on alumimumn oxides by the same mechanism that involves hydrolysis after adsorption. However, their study suggested that unhydrolyzed species can also adsorb. Saeki et al. found that Mn^{2+} irreversibly adsorbed to silica at pH > 6.0.[40]

As referenced above, most literature described metal cations as a function of hydrolysis although no consensus was presented on the direction of that effect. Noted discrepancies could have resulted from different experimental conditions e.g., pH and concentrations, and techniques and procedures used for measuring adsorption and formed surface complexes. Here we seek to conduct a systematic study of Cr^{3+}, Al^{3+} and Mn^{2+} adsorption onto SiO_2 and Al_2O_3 surfaces at an acidic pH (pH = 3.8 ± 0.2) using an integration of flow microcalorimetry (FMC) and quartz crystal microbalance with dissipation (QCM-D) measurements as well as density functional theory (DFT) calculations. Both FMC and QCM-D offer unique and complementary perspectives into adsorption processes due to the *in situ* and flow nature of their measurements, and DFT provides a framework to understand the experimental data. To our knowledge, this is the first time these three techniques are applied to the study of one system.

2. Experimental Section

2.1. Chemicals and solutions

All reagents and salts used were ACS grade chemicals. Anhydrous $NaNO_3$ was oven-dried overnight at 85 °C and all hydrated salts [$Al(NO_3)_3 \cdot 9H_2O$, $Cr(NO_3)_3 \cdot 9H_2O$, $Mn(NO_3)_2 \cdot 4H_2O$] were

used as received. $Me^{n+}(NO_3)_n$ (Me = Al^{3+}, Cr^{3+}, or Mn^2) solutions were prepared at a concentration of 1×10^{-3} M, in a background of 2.9×10^{-3} M $NaNO_3$ for microcalorimetry experiments. For QCM-D experiments, only Mn^{2+} solutions were prepared in a 2.9×10^{-3} M $NaNO_3$ (Table S1) to maintain the same ionic strength (I). A $NaNO_3$ solution was also prepared at a concentration of 2.9×10^{-3} M as a control. All solutions were prepared using ultrapure water ($\Omega > 18.2$ MΩ.cm) and were carefully adjusted to pH 3.8 ± 0.1 using dropwise addition of 1 M HNO_3 or 1 M NaOH. Inductively coupled plasma optical emission spectroscopy (ICP-OES) analysis of all solutions confirmed negligible changes to the total aqueous M^{n+} concentration due to this adjustment.

2.2. Flow Microcalorimetry (FMC) Experiments

Corundum (Al_2O_3) crystals were purchased from Wards' Scientific (Rochester, NY), cleaned and ground as per previously reported procedures.[42] The resulting powdered sample was fractionated through sequential sieving, and the fine fraction (< 35 μm) was collected for all microcalorimetry experiments. The SiO_2 sample used was obtained by grinding large pieces of single crystals of Brazilian quartz, separating the coarser fractions in methanol, followed by centrifuging and air drying the finer fraction. The sample was used and well characterized in a previous study.[43]

Experiments were performed using custom-designed flow microcalorimeters fabricated in the Kabengi laboratories at Georgia State University. The instrument design and experimental procedures have been thoroughly discussed in previous works.[43-46] To obtain the heats of cation adsorption ($Q_{ads\ in}$ mJ/mg), a known mass (~30.0 – 35.0 mg) of either Al_2O_3 or SiO_2 powder was packed into the sample holder and equilibrated with the $NaNO_3$ solution until a thermal baseline was established at 20 ± 0.1 °C. The input solution was then switched to a $M^{n+}(NO_3)_n$ solution and the calorimetric signal for the M^{n+} reaction with the surface was recorded (denoted [Na/M^{n+}]).

Once the reaction reached thermal equilibrium as defined by the return of the calorimetric signal to the initial baseline, the solution was returned to the $NaNO_3$ solution. The calorimetric signal associated with M^{n+} displacement from the surface (denoted [M^{n+}/Na]) and its corresponding [Na/M^{n+}] constituted one cycle, which was repeated 3-5 times for each $M^{n+}(NO_3)_n$ solution to establish statistically representative values. The reproducibility of the calorimetric peaks obtained was further used to assess the reversibility of the complexes formed by each cation. During both [Na/M^{n+}] and [M^{n+}/Na] cycles, the effluent samples were collected for chemical analysis. The amount of M^{n+} retained at or exchanged from the surface was determined by a mass balance calculation between the total mass injected and the mass recovered from effluent samples. The total aqueous concentration of Mn^{2+} and Cr^{3+} was determined using inductively coupled plasma optical emission spectroscopy (Varian 730-ES ICP-OES, Varian), and that of Al^{3+} by UV-Vis spectroscopy (GENESYS 10S, Thermo Scientific) using the catechol violet method.[47]

2.3. Quartz Crystal Microbalance with Dissipation (QCM-D) Measurements

Cation (Mn^{2+}, Al^{3+}, or Cr^{3+}) adsorption onto SiO_2 or Al_2O_3 substrates was also studied using QCM-D. Quartz sensors coated with SiO_2 (QSX 303) or Al_2O_3 (QSX 309) were purchased from Q-sense. For each cation adsorption experiment, a clean sensor was placed into the flow module with the SiO_2 or Al_2O_3 coating facing the solution. Then the flow module was placed on the chamber platform of QCM-D (Biolin Scientific, Paramus, NJ), and the temperature inside the flow module was maintained at 20 ± 0.1 °C. Initially, ultrapure water was pumped into the flow module at a constant rate of 0.2 mL/min to establish a stable baseline (Figures 1 and S1). Then the inflow solution was switched (indicated by arrows in Figures 1 and S1) to either one of $M^{n+}(NO_3)_n$ (with or without $NaNO_3$) or the control $NaNO_3$ solution.

Finally, the solution was switched back to ultrapure water (indicated by arrows in Figures 1 and S1), to test if the cations adsorbed on each substrate could be desorbed. The changes in resonance frequency (Δf) and energy dissipation (ΔD) of the sensors were recorded, and the mass changes (ng/cm^2) corresponding to the adsorption of the cations onto SiO_2 or Al_2O_3 coatings on the sensors were calculated using Sauerbrey model.[48] The measured mass change in ng/cm^2 is normalized by the geometric areas of Al_2O_3 or SiO_2 coatings on the QCM-D sensors and not the actual specific surface areas of Al_2O_3 or SiO_2 powders coated on the sensors as these are hard to measure. All data were analyzed by Q-Tools 3.0 from Biolin Scientific, and detailed information can be found in our previous publications.[42, 49-53]

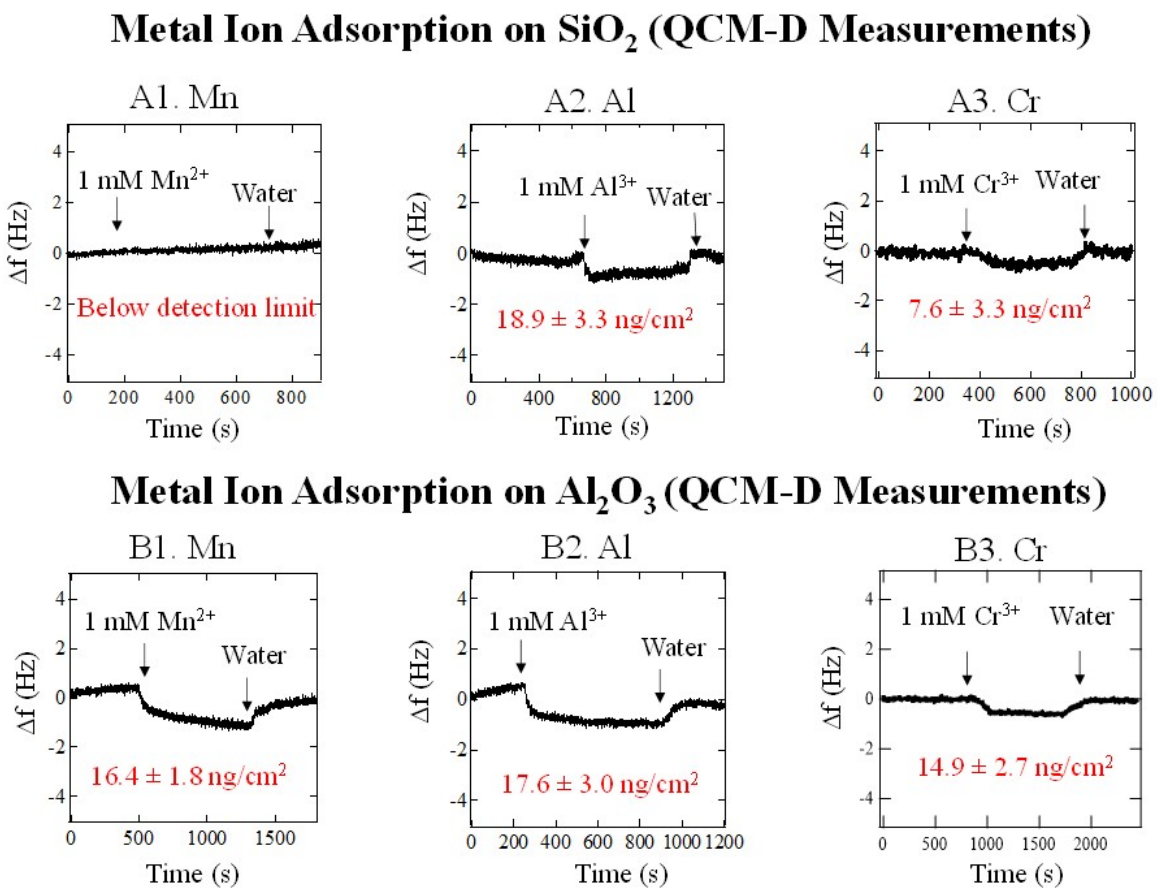

Figure 1: QCM-D measurements of Mn^{2+}, Cr^{3+}, and Al^{3+} ion adsorption onto SiO_2 (A1-A3) and Al_2O_3 sensors (B1-B3) at pH = 3.8 ± 0.2. To establish a stable baseline, measurements were conducted by flowing ultrapure water over SiO_2 and Al_2O_3 sensors. Then the solution was switched to 1 mM $Mn(NO_3)_2$ (with 2.9 mM $NaNO_3$ added to adjust the ionic strength), 1 mM $Al(NO_3)_3$, and 1 mM $Cr(NO_3)_3$ test solutions (the arrows indicate the switching points). The decreases in frequency (Δf) indicate the adsorption of ions onto SiO_2 and Al_2O_3 sensors. Finally, the inlet solution was switched back to ultrapure water, to test the reversibility of the ion adsorption on substrates (arrows indicate the switching points).

2.4. Density Functional Theory (DFT) Calculations

DFT calculations using Gaussian 09[54] were used to calculate the minimum energy structure, vibrational frequencies and bonding of simple molecular clusters representing adsorbed Mn^{2+}, Al^{3+}, and Cr^{3+} onto silanol and aluminol sites on SiO_2 and Al_2O_3. All models were constructed in a monodentate bonding configuration (Figure 2) assuming that Q^3 SiOH groups or $AlOH_2$ groups with 5 bonds to the bulk dominate the surfaces under study. This is likely to be the case for silica surfaces[55] although certain faces can be dominated by Q^2 SiOH groups. The $AlOH_2$ surface site is also thought to dominate most alumina surfaces at low pH[56] compared to geminal sites. Hydroxyl groups bonded to 2 or 3 Al surface atoms are generally considered less reactive towards H^+/Me^{n+} exchange.

The structures were drawn manually in the Visualizer module of Materials Studio 2016 (Biovia Inc., San Diego, CA).[57] Compositions included: $(OH)_3SiOSi(OH)_2O$-(Mn^{2+}, Al^{3+}, or Cr^{3+})•$5(H_2O)$ and $Al_2(OH)_6(H_2O)_3O$-(Mn^{2+}, Al^{3+}, or Cr^{3+})•$5(H_2O)$ which assumes no hydrolysis of the adsorbed metal ions. Hydrolyzed ion adsorption was modeled with the compositions $(OH)_3SiOSi(OH)_2O$-$Al(OH)_3(H_2O)_2$, $(OH)_3SiOSi(OH)_2O$-$Mn(OH)_2(H_2O)_3$, $(OH)_3SiOSi(OH)_2O$-$Cr(OH)_3(H_2O)_2$, $Al_2(OH)_6(H_2O)_3O$-$Al(OH)_3(H_2O)_2$, $Al_2(OH)_6(H_2O)_3O$- $Mn(OH)_2(H_2O)_3$, and $Al_2(OH)_6(H_2O)_3O$- $Cr(OH)_3(H_2O)_2$ (Figure S3). Spin states of Mn^{2+}, Al^{3+}, or Cr^{3+} were set to 5, 0, and 3, respectively (multiplicity of the corresponding models 6, 1 and 4).

Energy minimizations (i.e., structural optimizations) were performed using the DFT exchange-correlation functionals B3LYP[58, 59] and the 6-311+G(d,p) basis set.[60, 61] Energies were minimized to Gaussian 09 default values, then frequency analyses were performed to ensure that a minimum had been obtained. When the frequency analyses resulted in no imaginary (i.e., negative) frequencies, we concluded the structure was at least in a local potential energy surface minimum (Note: We make no claim that any structure is in the global minimum structure as extensive configurational searches were not performed). Natural population analyses[62] were performed on these structures to determine the strength and electron population of bonds in the cluster. The focus was on the metal ion bond to the O atom connecting to the Si or Al of the model surface cluster because this is the key bond that will be involved if a metal ion is adsorbed to a surface.

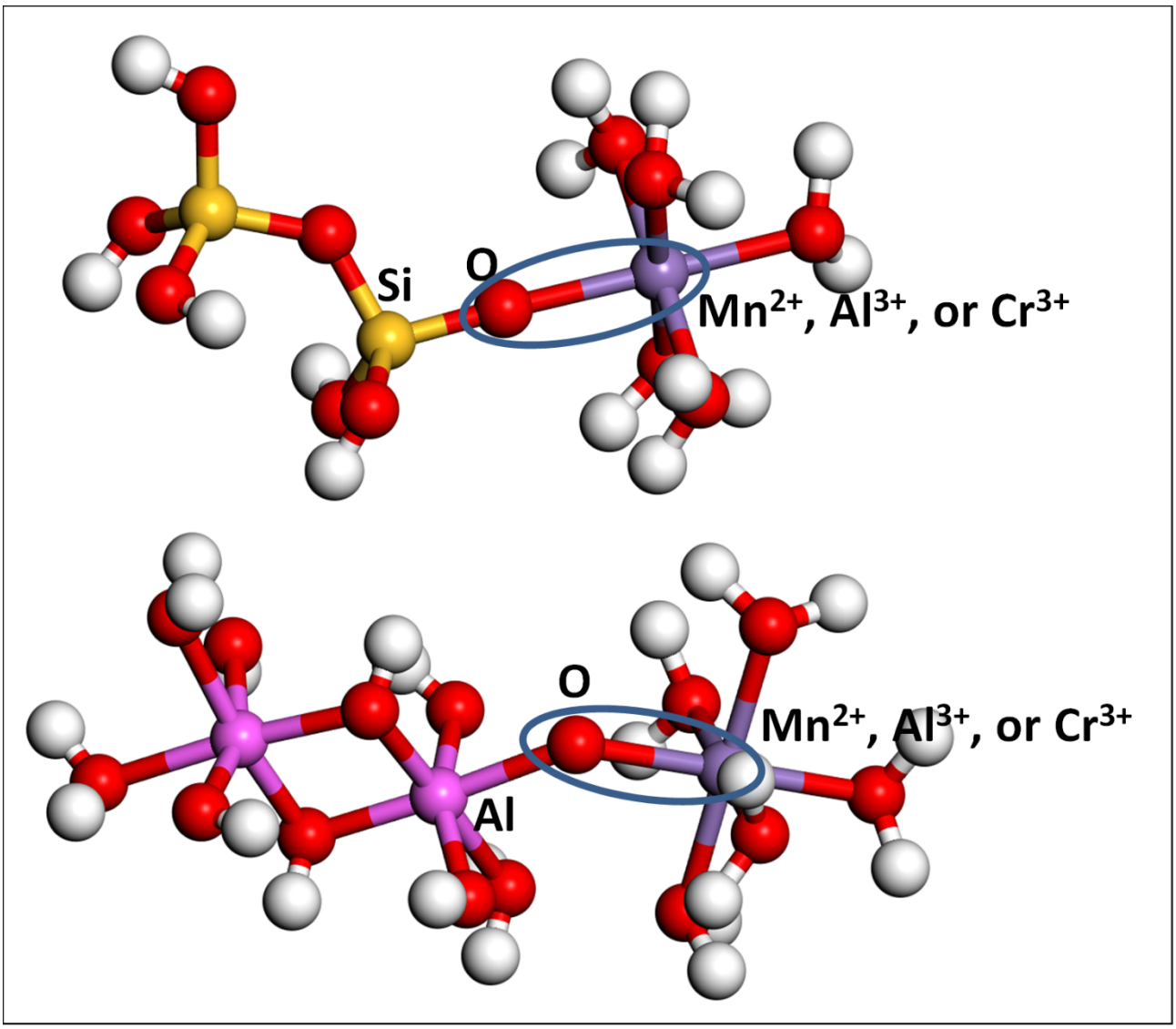

Figure 2: Fully hydrated models for adsorption of Mn^{2+}, Al^{3+}, and Cr^{3+} onto silanol and aluminol sites on quartz and corundum. All models were constructed in a monodentate bonding configuration assuming that Q^3 SiOH groups or $AlOH_2$ groups with 5 bonds to the bulk dominate the surfaces under study. The circled bond energy as calculated by NBO analysis is compared to the O-H bond it replaces (Table 2). (Si yellow, O red, H white, Al magenta, Mn and Cr purple)

3. Results and Discussion

3.1. Selective Cation Adsorption on SiO_2 and Al_2O_3

FMC and QCM-D experiments were conducted to measure Mn^{2+}, Al^{3+}, and Cr^{3+} adsorption on SiO_2 and Al_2O_3 surfaces. Figure 3 shows the calorimetric signal for the initial exposure of both Al_2O_3 and SiO_2 surfaces to the $M^{n+}(NO_3)_n$ solutions. The reaction of Al^{3+} with both surfaces was

found to be endothermic as evidenced by the negative peak (voltage decrease corresponding to a decrease in temperature); Cr^{3+} adsorption was exothermic on both surfaces albeit significantly smaller on SiO_2 than on Al_2O_3; whereas Mn^{2+} reaction was endothermic on Al_2O_3 and below detection limit on SiO_2.

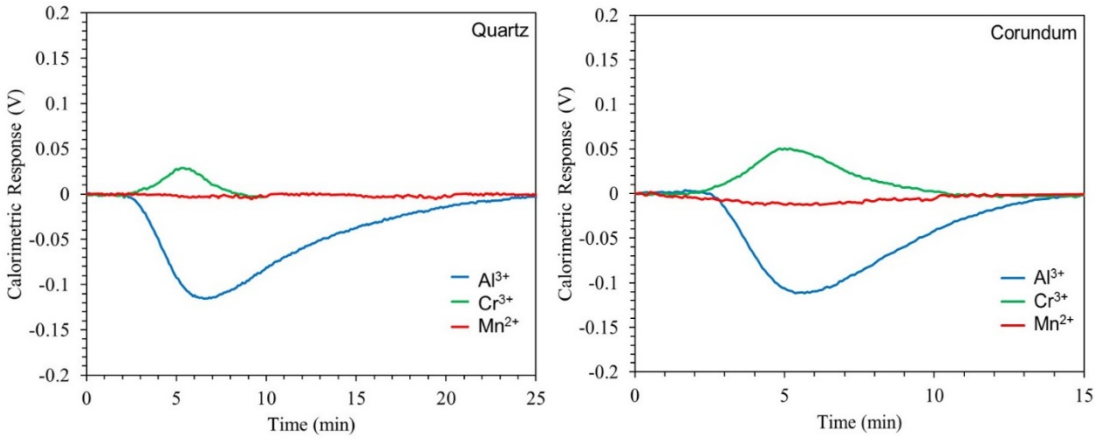

Figure 3: Calorimetric response to M^{n+} adsorption to SiO_2 and Al_2O_3. Positive calorimetric response corresponds to an exothermic process, while the negative calorimetric response corresponds to an endothermic process.

The adsorption of cations on the SiO_2 (Figure 1 A1-A3) and Al_2O_3 (Figure 1 B1-B3) substrates at pH = 3.8 ± 0.2 was also measured by QCM-D. The decreases in resonance frequency (Δf) indicated the increases of mass on sensors caused by cation adsorption. For the control experiment with 2.9 mM $NaNO_3$ solution (Figure S1 in Supporting Information), no changes in resonance frequency (Δf) were detected on SiO_2 and Al_2O_3 sensors, indicating that no significant adsorption of Na^+ or NO_3^- on SiO_2 and Al_2O_3 substrates occurred. Therefore, decreases in resonance frequency (Δf) of the sensors (Figure 1), while in contact with $Al(NO_3)_3$, $Cr(NO_3)_3$, and $Mn(NO_3)_2$ solutions, must be caused by the adsorption of Al^{3+}, Cr^{3+}, and Mn^{2+} ions on sensors.

Table 1: Metal cation adsorption onto substrates measured by QCM-D and their hydrolysis.

Sample Name	[1]$M^{n+}(OH)_n$,[a] %	M^{n+}, %	[2]M_SiO_2, ng/cm^2	[2]M_Al_2O_3, ng/cm^2
Mn	0.5	99.5	[3]BDL	16.4 ± 3.3
Al	4.4	95.6	18.9 ± 3.3	17.6 ± 3.0
Cr	78.7	21.3	7.6 ± 3.3	14.9 ± 2.7

[1]$M^{n+}(OH)_n$, [a],%: Percentages of metal ions in hydrolyzed states (e.g. $Al(OH)^{2+}$, $Al(OH)_2^+$, $Al(OH)_3$), which were calculated using Geochemist Work Bench (Release 9.0, Aqueous Solutions LLC) under our experimental conditions.
[2] M_SiO_2[b] and M_Al_2O_3[b]: the amounts of Mn^{2+}, Al^{3+}, and Cr^{3+} ions adsorbed on SiO_2 -and Al_2O_3- sensors, measured by QCM-D. No significant adsorption of 2.9 mM $NaNO_3$ on SiO_2 and Al_2O_3 coated quartz sensors was observed.
[3] BDL: below the detection limit of the instrument

On the SiO_2 sensor, no changes in resonance frequency (Δf) were recorded after switching from ultrapure water to $Mn(NO_3)_2$ solution, indicating no significant adsorption of Mn^{2+} on SiO_2. For $Al(NO_3)_3$ and $Cr(NO_3)_3$, ~ 1 Hz and ~ 0.3 Hz respective decreases in resonance frequency (Δf) were measured, indicating that 18.9 ± 3.3 ng/cm^2 Al^{3+} and 7.6 ± 3.3 ng/cm^2 Cr^{3+} cations were adsorbed. On the Al_2O_3 sensor, ~ 1 Hz decreases in vibrational frequency (Δf) were detected after switching to $Al(NO_3)_3$, $Cr(NO_3)_3$, and $Mn(NO_3)_2$ solutions. This indicated that all three cations can adsorb on Al_2O_3 substrates at pH = 3.8 ± 0.2, with similar amounts of 16.4 ± 3.3, 17.6 ± 3.0, and 14.9 ± 2.7 ng/cm^2, for Al^{3+}, Cr^{3+}, and Mn^2 respectively (Table 1). In summary, the ion adsorption behaviors measured by FMC and QCM-D were consistent at pH = 3.8 ± 0.2. Both techniques showed the selective adsorption of Al^{3+} and Cr^{3+} and the lack of adsorption of Mn^{2+} onto SiO_2. All three cations (Al^{3+}, Cr^{3+}, and Mn^{2+}) adsorbed on Al_2O_3 substrates.

3.2. Chemical Bond Formation During Ion Adsorption on Substrates

DFT calculations were conducted to obtain information on bond energies. Each of the clusters resulted in energy minima with no imaginary frequencies. The bond lengths predicted generally followed the observed bond lengths in minerals and aqueous species of the ions in

question. Although Gibbs free energies result from the frequency analyses of each cluster, we have no basis for comparison of these surface complex models to produce a ΔG of adsorption. Such a calculation would require modeling of the aqueous species and the model surface which is outside the scope of the current study. Consequently, we extracted the bond energies for the Mn-, Al-, and Cr-O bonds connecting the $Me^{n+}\bullet 5(H_2O)$ group to the silica and alumina clusters as well as the Si and Al surface to O bonds and compared the former to O-H bond energies and the Si-(OH) and Al-(OH_2) bonds each would be replacing. Lower bond energies than the original Si-(OH) and Al-(OH_2) were considered to favor adsorption via ligand exchange. If this mechanism was not favorable, then the potential for exchange of the cations with H^+ was considered by comparing to the original surface O-H bond.

The bond energies are listed in Table 2. For the fully hydrated models (i.e., 5 H_2Os on the adsorbing cation), most Me^{n+}-O_{Surf} bond energies are negative and fall in the range of approximately -71 to -101 kJ/mol which is reasonable for these metal ions to O atoms. A negative bond energy does not imply stability of the surface complex, however. For a surface complex to be thermodynamically stable on SiO_2, it should be lower in energy than the O-H bond it replaces on SiO_2 (e.g., SiO-H + Me^{n+} → SiO-Me^{n+} + H^+). Considering conditions where the [H^+] is greater than the [Me^{n+}] requires that the Me^{n+}-O bond be stronger (i.e., Le Châtelier's Principle). In this context, in the fully hydrated SiO_2 cluster, the bond energies in Table 2 for the O-Al^{3+} and O-Cr^{3+} bonds are significantly lower in energy (-101 and -96 kJ/mol, respectively) than the original O-H (-74 kJ/mol). Exchange of the Al^{3+} and Cr^{3+} for H^+ at SiOH sites is therefore possible. No covalent Mn^{2+}-O_{Surf} bond was determined in the NBO analysis for the $(OH)_3SiOSi(OH)_2O$-$Mn^{2+}\bullet 5(H_2O)$ model; hence, no energy of this bond could be determined. These bond energies are qualitatively consistent with the calorimetry and QCM-D measurements that the adsorption of Mn^{2+} on SiO_2 is

negligible; whereas, the adsorption of Al^{3+} and Cr^{3+} on SiO_2 was significant. The results are consistent with exchange of the Al^{3+} and Cr^{3+} for H^+ at SiOH.

Table 2: Calculated metal-oxygen (O-H) bond energies for model adsorption complexes.

Model	Energy (kJ)	
	Me^{n+}-O_{Surf}	Surf-O(Me^{n+})
$S(OH)_3SiOSi(OH)_2$-OH	----	-85
$(OH)_3SiOSi(OH)_2O$-H	-74	----
$(OH)_3SiOSi(OH)_2O$-Al^{3+}•5(H_2O)	-101	-101
$(OH)_3SiOSi(OH)_2O$-Cr^{3+}•5(H_2O)	-99	-96
$(OH)_3SiOSi(OH)_2O$-Mn^{2+}•5(H_2O)	No covalent bond	-97
$(OH)_3SiOSi(OH)_2O$-$Al(OH)_3(H_2O)_2$	-59	-68
$(OH)_3SiOSi(OH)_2O$-$Cr(OH)_3(H_2O)_2$	-55	-67
$(OH)_3SiOSi(OH)_2O$-$Mn(OH)_2(H_2O)_3$	No covalent bond	-72
$Al_2(OH)_6(H_2O)_3$-OH_2	----	-69
$Al_2(OH)_6(H_2O)_3O$-H_2	-64	----
$Al_2(OH)_6(H_2O)_3O$-Al^{3+}•5(H_2O)	-81	-76
$Al_2(OH)_6(H_2O)_3O$-Cr^{3+}•5(H_2O)	-71	-85
$Al_2(OH)_6(H_2O)_3O$-Mn^{2+}•5(H_2O)	-77	No covalent bond
$Al_2(OH)_6(H_2O)_3O$-$Al(OH)_3(H_2O)_2$	-49	-51
$Al_2(OH)_6(H_2O)_3O$-$Cr(OH)_3(H_2O)_2$	-39	-48
$Al_2(OH)_6(H_2O)_3O$-$Mn(OH)_2(H_2O)_3$	-34	-39

For the fully hydrated models of Al_2O_3 complexes, Al^{3+}, Cr^{3+}, and Mn^{2+} are all predicted by DFT (Table 2) to have lower energy bonds to the alumina surface O atom (i.e., -81, -71, and -77 kJ/mol) than one (Al)O-H bond (-64 kJ/mol) but not compared to double deprotonation of Al-OH_2 (≈ -128 kJ/mol). The Al^{3+} and Cr^{3+} bonds to the surface O atom are calculated to be lower in energy than an Al-OH_2 bond (-76 and -85 compared to -69 kJ/mol, Table 2). Hence, Al^{3+}, Cr^{3+}, and Mn^{2+} could exchange with an H^+, and Al^{3+} and Cr^{3+} could undergo ligand exchange with an Al-OH_2. The results are consistent with the observations of adsorption of all three cations to the alumina surface, but these possible mechanisms could be better explored with periodic DFT calculations that better account for the mineral-water interface structure

3.3. The Role of Cation Hydrolysis in Adsorption Favorability

The metal-oxygen chemical bond energies calculated by DFT explained the selective cation itself adsorption on quartz and corundum from their chemical bonding formation with substrates under acidic condition. As discussed earlier, metal cation adsorption has been widely

reported to be a function of the cation hydrolysis.[63-65] Based on James and Healy model, hydrolyzed cations have lower charge and less strongly bounded water molecules, thus their adsorption is more favorable because of decreased ion-solvent interactions. Therefore, the model suggested that the mineral surfaces with a low dielectric constant (e.g., SiO_2) can adsorb hydrolyzed cations preferably over unhydrolyzed cations; whereas mineral surfaces with higher dielectric constants (e.g., TiO_2), can adsorb both hydrolyzed and unhydrolyzed cations.[63]

Because hydrolysis and coordination change may accompany adsorption for ions that undergo hydrolysis in solution,[66] model hydrolyzed surface complexes $(OH)_3SiOSi(OH)_2O$-$Al(OH)_3(H_2O)_2$, $(OH)_3SiOSi(OH)_2O$-$Mn(OH)_2(H_2O)_3$, and $(OH)_3SiOSi(OH)_2O$-$Cr(OH)_3(H_2O)_2$ (Figure 4) were examined. In this case, the Me^{n+}-O_{Surf} bonds of interest were all less energetically favored than the original (Si)O-H and (Al)O-H bonds (Table 2). This is expected because the metal-$(OH)_n$ bonds in the hydrolyzed species are stronger than metal-(OH_2) bonds which weakens the remaining Me^{n+}-O_{Surf} bond.

Natural bond orbital analysis[62] reveals a special case for the Si-O-Mn linkage, however, where no covalent bond is formed when the Mn^{2+} ion is hydrolyzed in $(OH)_3SiOSi(OH)_2O$-$Mn(OH)_2(H_2O)_3$ (Table 2; Figure 4). We also note that there is no covalent bond determined between the Al-O_{surf} in the $Al_2(OH)_6(H_2O)_3O$-Mn^{2+}•$5(H_2O)$ species, but in this case there is a Mn^{2+}-O_{surf} bond (Table 2), so adsorption would still be predicted as observed.

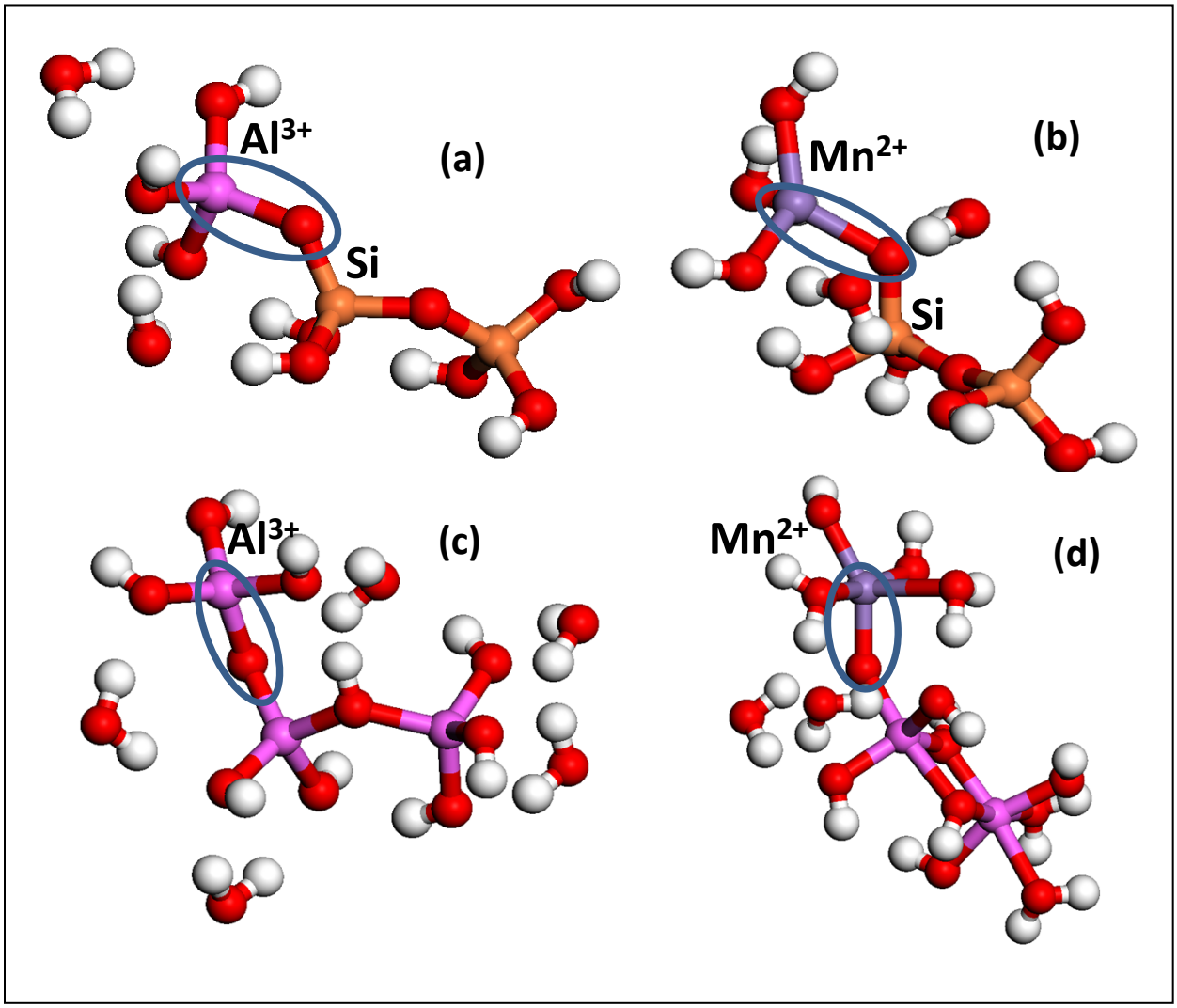

Figure 4: Hydrolyzed ion adsorption on quartz and corundum modeled with the compositions (a) $(OH)_3SiOSi(OH)_2O$-$Al(OH)_3(H_2O)_2$, (b) $(OH)_3SiOSi(OH)_2O$-$Mn(OH)_2(H_2O)_3$, (c) $Al_2(OH)_6(H_2O)_3O$-$Al(OH)_3(H_2O)_2$, and (d) $Al_2(OH)_6(H_2O)_3O$-$Mn(OH)_2(H_2O)_3$. Spin states of Mn^{2+}, Al^{3+}, or Cr^{3+} were set to 5, 0, and 3, respectively. The circled bond energy as calculated by NBO analysis is compared to the O-H bond it replaces (Table 2). (Si orange, O red, H white, Al magenta, Mn purple)

These hydrolyzed species ($Al(OH)_3$, $Cr(OH)_3$ and $Mn(OH)_2$) are end-members possible surface complexes in contrast to the other end-member fully hydrated models discussed above. Actual adsorbed species will likely fall between these two end-members and the species will

change with pH of the solution. Because both the fully hydrated and fully hydrolyzed Mn^{2+} model surface complexes resulted in the weakest interactions with the model silica surface, we concluded that bond energetics could explain the lack of Mn^{2+} adsorption onto SiO_2 in the QCM-D and FMC experiments. This was not the case for the Mn^{2+} surface complex model with the alumina cluster, so adsorption onto alumina should be favored for all the ions considered as measured experimentally.

Early work in the field of metal cation adsorption, in particular the James and Healy model,[67] defined adsorption through the lens of hydrolysis, whereas either hydrolyzed species adsorb more favorably or species underwent hydrolysis during adsorption as we also cite in the introduction. However, the prominent role of hydrolysis in adsorption was not supported by results from this study. As seen in Table 1, two of the cations studied, Al^{3+} and Mn^{2+}, did not significantly hydrolyze at the pH studied. The strong interactions of Al^{3+} with the mineral surfaces, seen both by FMC and QCM-D, suggested that this cation can adsorb to the mineral surface without a significant hydrolysis, at least at pH values at or below 3.8. Furthermore, the DFT results comparing the adsorption of hydrolyzed and unhydrolyzed cations showed a significant preference for the unhydrolyzed Al^{3+} ion, albeit only the extreme case of full hydrolysis was analyzed. Mn^{2+} adsorption occurred only on the Al_2O_3 surface, and not on the SiO_2 surface. This finding was seen in both QCM-D and FMC results. The DFT calculations showed that a SiO_2- Mn^{2+} bond was not favorable, regardless of the hydrolysis state. On the other hand, the Cr^{3+} interactions with both SiO_2 and Al_2O_3 suggested that Cr^{3+} was forming a covalent bond with the surface, a significantly different interaction from the electrostatic adsorption for the other cations. This was because that the ability of Cr^{3+} to form this covalent bond with the surface is due, in part, to its hydrolyzed state. This suite of markedly different interactions demonstrated that adsorption studies of cations in

acidic conditions needed to take into consideration all cation species. Adsorption may occur as a variety of complexes depending upon solution conditions.

3.4. The Reversibility of Cation Adsorption

The reversibility of the adsorption of each cation was also explored using both FMC and QCM-D. In FMC experiments, the reversibility was determined by comparing Q_{ads} (Table 3) of the initial interaction with those obtained during subsequent adsorption-desorption cycles. The reversibility of the Mn^{2+} could not be analyzed due to its low Q_{ads} on Al_2O_3 (0.008 ± 0.004 mJ/mg, Table 3) and the absence of any detectable Q_{ads} on SiO_2. The adsorption and desorption of Al^{3+} was found to be nearly completely reversible on both SiO_2 and Al_2O_3, with minimal changes in the calorimetric signal over consecutives cycles (Table 3). The adsorption of Cr^{3+} exhibited a more complex and partially reversible behavior. On SiO_2, compared with the initial Cr^{3+} adsorption, there was a 65% decrease in the Q_{ads} during the second exposure (Table 3). We attributed this reduction to the inability of $NaNO_3$ to exchange the initial Cr^{3+} off the surface. This was further confirmed by the smaller size of the [Cr^{3+}/Na^+] calorimetric peak obtained following the initial Cr^{3+} exposure (data not shown). On Al_2O_3, Cr^{3+} adsorption was found to be even less reversible, with 80% reduction in Q_{ads} of the second [Na^+/Cr^{3+}] cycle (Table 3).

Table 3: Determination of the reversibility of metal cation adsorption using flow microcalorimetry.

Cation	Q_{ads} (in mJ/mg)	Al_2O_3	SiO_2
Al^{3+}	Initial	+0.201	+0.297
	Following	+0.183 (0.006[1])	+0.296 (0.030)
	% Change[2]	9%[3]	<1%
Cr^{3+}	Initial	-0.065	-0.032
	Following	-0.013 (0.006)	-0.011 (0.003)
	% Change	80%	65%

[1]The values in parentheses correspond to the standard error
[2]% Change was calculated as ([Initial – Subsequent)/Initial] × 100).
[3]Low values for % change correspond to highly reversible interactions while high values correspond to more irreversible interactions

The change in the heat, or lack thereof, can be used to gain insights into the strength and mode of binding of the cation with the mineral surface. As discussed in Cao et al.,[68] Sabur et al.,[69] and Kabengi et al.,[45, 70] for anions, a change in sequentially repeated heat measurements for ion interaction with mineral surfaces can be attributed to irreversible processes such as complexation or precipitation, while unchanged heats over repeated measurements correspond to reversible reactions that are dominated by electrostatic interactions. As such, the observed irreversible Cr^{3+} adsorption behavior suggested a strong surface interaction with SiO_2 and Al_2O_3, similar to those described by Cao et al.[68] while the reversible adsorption of Al^{3+} suggested electrostatic interaction with the SiO_2 and Al_2O_3 surface.

In QCM-D measurements, the reversibility was assessed by measuring the changes in vibrational frequency (Δf) of sensors during the desorption experiments, i.e., after the inlet solutions were switched back from the cation-containing solutions to ultrapure water (indicated by arrows in Figure 1). For both SiO_2 and Al_2O_3 sensors, for all three cations the vibrational frequencies went back to the original baselines established in ultrapure water (Figure 1), indicating that the adsorbed cations can be desorbed from the substrates in ultrapure water and hence their adsorption is completely reversible. The discrepancy between FMC and QCM-D assessment of reversibility of Cr^{3+} could be due to differences in the protocols of the desorption experiments. First, $NaNO_3$ solution and ultrapure water were used for desorption during FMC and QCM-D measurements, respectively. Second, powders of quartz and corundum crystals were used to conduct FMC measurement, while amorphous SiO_2 and Al_2O_3 powders coated on quartz sensors were used in QCM-D measurements.

3.5. The Roles of Cation Hydrolysis and Dehydration in Adsorption Enthalpy and Reversibility

Our measurements showed that Al^{3+} can adsorb on both surfaces with complete reversibility; Cr^{3+} can adsorb on both surfaces with partial reversibility; and Mn^{2+} can only adsorb onto Al_2O_3 and its adsorption is reversible. The differences in cation adsorption on substrates and the adsorption reversibility could be indicative of their different interactions with the substrates. It has been suggested recently that most cations undergo a partial dehydration before adsorbing onto a mineral surface[71-74] through inner-sphere binding mode. Furthermore, the relationship between cation dehydration and the heats of cation interactions was established[43, 46, 75] for alkali and alkaline earth, and other multivalent cations (Cd^{2+}, Co^{2+}, Zn^{2+}, Eu^{3+}). In particular, Hawkins et al.[46] and Allen et al.[43] demonstrated that the endothermic heats measured during cation adsorption were primarily a function of the bulk dehydration enthalpy. As such, it is a reasonable assertion that the endothermic heats measured for both Mn^{2+} and Al^{3+} adsorption could also be a function of a partial dehydration step as seen in equation 1.

Equation 1: $$>S-O^- + Me(H_2O)_6^{n+} \rightarrow >S-O\cdots Me(H_2O)_5^{n+} + H_2O$$

Where >S is a representative surface functional group, Me is a metal cation, and n corresponds to the charge on the cation.

On another hand, the exothermic heat measured during the Cr^{3+} adsorption alludes to a different adsorption mechanism. As seen from the reversibility analysis above, Cr^{3+} interaction with the surface is partially irreversible, suggesting that it is forming a stronger interaction with the surface, potentially as an inner-sphere complex or covalent bond as discussed in the DFT section. To make such a bond, Cr^{3+} would first need to partially dehydrate to attain a point close enough to the surface to form the bond. Hence, the expected measured heat would be the net summation of the dehydration energy (endothermic process) and the bond formation energy (exothermic process). The energy of a Cr-O bond formation is tabulated at -461 kJ/mol[76] whereas

the bulk hydration enthalpy (ΔH_{hyd}) of Cr^{3+} is -4560 kJ/mol[77]. A H_2O loss from the hydration shell can then be roughly approximated to release ~ +760 kJ/mol (bulk hydration enthalpy/coordination number of 6).[46] Therefore, the measured heat should still be a net endothermic reaction. But as seen in Table 1 and Figure 4, under our experimental conditions, a sizable percentage of Cr^{3+} exists in a hydrolyzed state, $Cr(OH)^{2+}$ and the trimer $Cr_3(OH)_4^{5+}$, and hence the bonds between the cation and the remaining H_2O molecules are much weaker and have a lower dehydration energy.[78] In this case, the net measured heat for Cr^{3+} adsorption will become exothermic, as found experimentally.

Although the bulk solution was undersaturated with respect to $Cr(OH)_3$, the surface precipitation of amorphous chromium hydroxide ($Cr(OH)_3$) on the mineral surface must be also considered as a possibility to explain the interaction of the Cr^{3+} with the mineral surfaces. However, a precipitation is expected to be endothermic (+110.5 kJ/mol)[79] and this would have been detected calorimetrically. Furthermore, since the net energy measured was exothermic a significant surface precipitation reaction was ruled out.

4. Conclusions

This work combined FMC, QCM-D, and DFT to examine the interactions of three metal cations (Al^{3+}, Cr^{3+}, and Mn^{2+}) and their hydrolyzed states ($M_n(OH)^{n+}$) with SiO_2 and Al_2O_3 surfaces under acidic pH condition (pH ~ 3.8) by systematically investigating their selective adsorption and reversibility, reaction energetics, and bond energy. QCM-D and FMC experiments showed that the cations could adsorb onto both surfaces with the exception of Mn^{2+} onto the SiO_2 surface. FMC determined that Mn^{2+} adsorption on Al_2O_3 was endothermic, the adsorption of Al^{3+} on both surfaces was endothermic and completely reversible, and the adsorption of Cr^{3+} on both surfaces was exothermic and partially reversible (65% on SiO_2 and 80% on Al_2O_3). The selective

adsorption of these cations onto SiO_2 and Al_2O_3 surfaces was rationalized by comparing bond energies between the adsorbed cations and SiO_2/Al_2O_3 to the Si-(OH) and Al-(OH) bonds each would be replacing during adsorption. DFT calculations showed that Mn^{2+}-SiO_2 bond is not favorable over Si-(OH) whereas the bond energies for adsorbed Cr^{3+} and Al^{3+} on both surfaces and Mn on Al_2O_3, were lower than the Si-(OH) and Al(-OH). In all instances, DFT agreed with experimental results.

The underlying mechanisms were further revealed through the enthalpic sign and reversibility of the adsorption of each cation. The endothermic heat measured for Mn^{2+} adsorption on Al_2O_3 and Al^{3+} adsorption on both surfaces indicated that their adsorption involved dehydration while the complete reversibility of the adsorption pointed out to the formation of weak electrostatic interactions. The exothermic and partially irreversible adsorption of Cr^{3+} with SiO_2 and Al_2O_3 was believed to indicate the formation of inner-sphere complexes or covalent bonds as opposed to $Cr(OH)_3$ precipitates which would have been endothermic. Cr^{3+} was thought to exhibit a different adsorption mechanism due to hydrolysis, in that at pH 3.8 a large percentage (78.7%) of Cr^{3+} exists as hydrolyzed specie which lowered the energy cost of dehydration resulting in an exothermic reaction. Furthermore, the favored covalent bond formation between hydrolyzed Cr species and the surface resulted in a partially irreversible adsorption.

This study provided new insights on the roles of ion hydration/dehydration and hydrolysis on cation adsorption whereby the latter favored specific adsorption by lowering the energy cost of dehydration. The dielectric constants of quartz and corundum studied here did not vary enough to observed markedly different results. Further work will encompass surfaces with even high dielectric constant, e.g., rutile (ε=18.2) or anatase (ε = 121).

Our study presented a modeling "shortcut" to rationalizing experimental adsorption data obtained from both FMC and QCM-D. The relatively quick and qualitative method uses bond energies as a guide to indicate the possibility of thermodynamically favored adsorption. The strong agreement between DFT and the experimental techniques suggests the new method to be an exciting and viable approach for the study of other potentially more complex adsorption systems.

Acknowledgements

This material is based upon work supported by the U.S. Department of Energy (DOE), Office of Science, Office of Basic Energy Sciences, Chemical Sciences, Geosciences, and Biosciences Division (Geosciences Program). N.A and N.K. were funded under Award Number DE-SC0012186.

N.A and N.K. would like to thank David Wesolowski, Michael Machesky, and Kathryn Grant for reading and making comments on the document. The computational work was made possible via the Research and Academic Data Center at the University of Texas at El Paso.

Supporting Information Available

Discussion on the reversibility experiments, Table of QCM-D experimental conditions (Table S1), QCM-D control measurements of Na^+ and NO_3^- ion adsorption onto SiO_2 (Figure S1), Figures showing DFT models (Figure S2-S3), and speciation diagrams for the cations analyzed (Figure S4). This material is available free of charge via the Internet at http://pubs.acs.org.

References

1. Kochian, L. V., Cellular Mechanisms of Aluminum Toxicity and Resistance in Plants. *Annual Review of Plant Physiology and Plant Molecular Biology* 1995, *46*, (1), 237-260.

2. Burrows, W. D.; Hem, J. D., Aquatic aluminum: Chemistry, toxicology, and environmental prevalence. *C R C Critical Reviews in Environmental Control* 1977, *7*, (2), 167-216.

3. Cronan, C. S.; Schofield, C. L., Relationships between aqueous aluminum and acidic deposition in forested watersheds of North America and northern Europe. *Environmental Science & Technology* 1990, *24*, (7), 1100-1105.

4. Cismasu, A. C.; Michel, F. M.; Stebbins, J. F.; Levard, C.; Brown, G. E., Jr., Properties of impurity-bearing ferrihydrite I. Effects of Al content and precipitation rate on the structure of 2-line ferrihydrite. *Geochim. Cosmochim. Acta* 2012, *92*, 275-291.

5. McBride, M. B., Trace and Toxic Elements in Soils. In *Environmental Chemistry of Soils*, Oxford University Press: New York, 1994; pp 308-341.

6. Tang, R.; Dai, C.; Li, C.; Liu, W.; Gao, S.; Wang, C., Removal of methylene blue from aqueous solution using agricultural residue walnut shell: equilibrium, kinetic, and thermodynamic studies. *Journal of Chemistry* 2017, *2017*.

7. Zhao, J.; Giammar, D. E.; Pasteris, J. D.; Dai, C.; Bae, Y.; Hu, Y., Formation and aggregation of lead phosphate particles: Implications for lead immobilization in water supply systems. *Environmental science & technology* 2018, *52*, (21), 12612-12623.

8. Smith, J. t.; Bailey, S., Second review of Al–O and Si–O tetrahedral distances. *Acta Crystallogr.* 1963, *16*, (8), 801-811.

9. Gao, X.; Hu, Y.; Li, C.; Dai, C.; Li, L.; Ou, X.; Wang, Y., Evaluation of fluorine release from air deposited coal spoil piles: A case study at Yangquan city, northern China. *Science of the Total Environment* 2016, *545*, 1-10.

10. Dove, P. M.; Han, N.; De Yoreo, J. J., Mechanisms of Classical Crystal Growth Theory Explain Quartz and Silicate Dissolution Behavior. *Proceedings of the National Academy of Sciences* 2005, *102*, (43), 15357-15362.

11. Kubicki, J. D.; Sofo, J. O.; Skelton, A. A.; Bandura, A. V., A New Hypothesis for the Dissolution Mechanism of Silicates. *The Journal of Physical Chemistry C* 2012, *116*, (33), 17479-17491.

12. Lanzl, C. A.; Baltrusaitis, J.; Cwiertny, D. M., Dissolution of Hematite Nanoparticle Aggregates: Influence of Primary Particle Size, Dissolution Mechanism, and Solution pH. *Langmuir* 2012, *28*, (45), 15797-15808.

13. Davies, S. H. R.; Morgan, J. J., Manganese(II) oxidation kinetics on metal oxide surfaces. *Journal of Colloid and Interface Science* 1989, *129*, (1), 63-77.

14. Hering, J. G., Stumm, W., Oxidative and Reductive Dissolution. In *Mineral-Water Interface Geochemistry*, Hochella. Michael F., W., Art F., Ed. Mineralogical Society of America: Washington, D.C., 1990; Vol. 23, pp 427-549.

15. Goldberg, S.; Criscenti, L. J.; Turner, D. R.; Davis, J. A.; Cantrell, K. J., Adsorption–Desorption Processes in Subsurface Reactive Transport Modeling. *Vadose Zone Journal* 2007, *6*, (3), 407.

16. Smith, K. S., Metal Sorption on Mineral Surfaces: An Overview with Examples Relating to Mineral Deposits. In *Reviews in Economic Geology*, Plumlee, G. S.; Lodgsdon,

M. J., Eds. Society of Economic Geologists, Inc.: Chelsea, Michigan, 1999; Vol. 6A, pp 161-182.
17. Liu, J.; Wu, X.; Hu, Y.; Dai, C.; Peng, Q.; Liang, D., Effects of Cu (II) on the Adsorption Behaviors of Cr (III) and Cr (VI) onto Kaolin. *J. Chem.* 2016, *2016*, 1-11.
18. Liu, J.; Dai, C.; Hu, Y., Aqueous aggregation behavior of citric acid coated magnetite nanoparticles: Effects of pH, cations, anions, and humic acid. *Environ. Res.* 2018, *161*, 49-60.
19. Hiemstra, T.; Venema, P.; Riemsdijk, W. H. V., Intrinsic Proton Affinity of Reactive Surface Groups of Metal (Hydr)oxides: The Bond Valence Principle. *Journal of Colloid and Interface Science* 1996, *184*, (2), 680-692.
20. James, R. O.; Healy, T. W., Adsorption of hydrolyzable metal ions at the oxide—water interface. I. Co(II) adsorption on SiO2 and TiO2 as model systems. *Journal of Colloid and Interface Science* 1972, *40*, (1), 42-52.
21. Michael, H. L.; Williams, D. J. A., Electrochemical Properties of Quartz. *Journal of Electroanalytical Chemistry and Interfacial Electrochemistry* 1984, *179*, (1), 131-139.
22. Duval, Y.; Mielczarski, J. A.; Pokrovsky, O. S.; Mielczarski, E.; Ehrhardt, J. J., Evidence of the Existence of Three Types of Species at the Quartz−Aqueous Solution Interface at pH 0−10: XPS Surface Group Quantification and Surface Complexation Modeling. *The Journal of Physical Chemistry B* 2002, *106*, (11), 2937-2945.
23. Kosmulski, M., Compilation of PZCs/IEPs. In *Surface Charging and Points of Zero Charge*, Hubbard, A. T., Ed. CRC Press: Boca Raton, FL, 2009; Vol. 145, pp 374-431.
24. Zhang, C.; Dai, C.; Zhang, H.; Peng, S.; Wei, X.; Hu, Y., Regeneration of mesoporous silica aerogel for hydrocarbon adsorption and recovery. *Marine pollution bulletin* 2017, *122*, (1-2), 129-138.
25. Levin, I.; Brandon, D., Metastable Alumina Polymorphs: Crystal Structures and Transition Sequences. *Journal of the American Ceramic Society* 1998, *81*, (8), 1995-2012.
26. Ates, M.; Demir, V.; Arslan, Z.; Daniels, J.; Farah, I. O.; Bogatu, C., Evaluation of alpha and gamma aluminum oxide nanoparticle accumulation, toxicity, and depuration in Artemia salina larvae. *Environmental Toxicology* 2015, *30*, (1), 109-118.
27. Sverjensky, D. A., Prediction of Surface Charge on Oxides in Salt Solutions: Revisions for 1:1 (M+L−) Electrolytes. *Geochimica et Cosmochimica Acta* 2005, *69*, (2), 225-257.
28. Nightingale, E. R., Phenomenological Theory of Ion Solvation. Effective Radii of Hydrated Ions. *J. Phys. Chem.* 1959, *63*, (9), 1381-1387.
29. Stumm, W.; Morgan, J. J., *Aquatic chemistry; an introduction emphasizing chemical equilibria in natural waters*. 1970.
30. Kuan, W. H.; Lo, S. L.; Wang, M. K., Modeling and electrokinetic evidences on the processes of the Al(III) sorption continuum in SiO2(s) suspension. *Journal of Colloid and Interface Science* 2004, *272*, (2), 489-497.
31. Bloom, P.; McBride, M.; Chadbourne, B., Adsorption of Aluminum by a Smectite: I. Surface Hydrolysis During Ca^{2+}-Al^{3+} Exchange 1. *Soil Sci. Soc. Am. J.* 1977, *41*, (6), 1068-1073.
32. Walker, W. J.; Cronan, C. S.; Patterson, H. H., A kinetic study of aluminum adsorption by aluminosilicate clay minerals. *Geochimica et Cosmochimica Acta* 1988, *52*, (1), 55-62.

33. Wehrli, B.; Ibric, S.; Stumm, W., Adsorption kinetics of vanadyl (IV) and chromium (III) to aluminum oxide: Evidence for a two-step mechanism. *Colloids and Surfaces* 1990, *51*, (Supplement C), 77-88.
34. Charlet, L.; Manceau, A. A., X-ray absorption spectroscopic study of the sorption of Cr(III) at the oxide-water interface: II. Adsorption, coprecipitation, and surface precipitation on hydrous ferric oxide. *Journal of Colloid and Interface Science* 1992, *148*, (2), 443-458.
35. Fendorf, S. E.; Lamble, G. M.; Stapleton, M. G.; Kelley, M. J.; Sparks, D. L., Mechanisms of chromium(III) sorption on silica. 1. Chromium(III) surface structure derived by extended x-ray absorption fine structure spectroscopy. *Environmental Science & Technology* 1994, *28*, (2), 284-289.
36. Fendorf, S. E.; Sparks, D. L., Mechanisms of chromium(III) sorption on silica. 2. Effect of reaction conditions. *Environmental Science & Technology* 1994, *28*, (2), 290-297.
37. Csobán, K.; Párkányi-Berka, M.; Joó, P.; Behra, P., Sorption experiments of Cr(III) onto silica. *Colloids and Surfaces A: Physicochemical and Engineering Aspects* 1998, *141*, (3), 347-364.
38. Bleam, W. F.; McBride, M. B., Cluster formation versus isolated-site adsorption. A study of Mn(II) and Mg(II) adsorption on boehmite and goethite. *Journal of Colloid and Interface Science* 1985, *103*, (1), 124-132.
39. Kerdpin, U.; Arquero, O.; Watanesk, R.; Sriyotha, U., Manganese(II) Adsorption Studies on Aluminum Oxide and Iron(III) Oxide by Neutron Activation Analysis. *Journal of the Science Society of Thailand* 1998, *24*, 73-80.
40. Saeki, K., Adsorption of Fe^{2+} and Mn^{2+} on silica, gibbsite, and humic acids. *Soil science* 2004, *169*, (12), 832-840.
41. Hachiya, K.; Sasaki, M.; Saruta, Y.; Mikami, N.; Yasunaga, T., Static and kinetic studies of adsorption-desorption of metal ions on a. gamma.-alumina surface. 1. Static study of adsorption-desorption. *J. Phys. Chem.* 1984, *88*, (1), 23-27.
42. Dai, C.; Liu, J.; Hu, Y., Impurity-bearing ferrihydrite nanoparticle precipitation/deposition on quartz and corundum. *Environmental Science: Nano* 2018, *5*, (1), 141-149.
43. Allen, N.; Machesky, M. L.; Wesolowski, D. J.; Kabengi, N., Calorimetric study of alkali and alkaline-earth cation adsorption and exchange at the quartz-solution interface. *Journal of Colloid and Interface Science* 2017, *504*, 538-548.
44. Rhue, R.; Appel, C.; Kabengi, N., Measuring surface chemical properties of soil using flow calorimetry 1. *Soil science* 2002, *167*, (12), 782-790.
45. Kabengi, N. J.; Chrysochoou, M.; Bompoti, N.; Kubicki, J. D., An integrated flow microcalorimetry, infrared spectroscopy and density functional theory approach to the study of chromate complexation on hematite and ferrihdyrite. *Chemical Geology* 2017, *464*, 23-33.
46. Hawkins, T.; Allen, N.; Machesky, M. L.; Wesolowski, D. J.; Kabengi, N., Ion Exchange Thermodynamics at the Rutile–Water Interface: Flow Microcalorimetric Measurements and Surface Complexation Modeling of Na–K–Rb–Cl–NO3 Adsorption. *Langmuir* 2017, *33*, (20), 4934-4941.
47. Dougan, W. K.; Wilson, A. L., The absorptiometric determination of aluminium in water. A comparison of some chromogenic reagents and the development of an improved method. *Analyst* 1974, *99*, (1180), 413-430.

48. Ekholm, P.; Blomberg, E.; Claesson, P.; Auflem, I. H.; Sjöblom, J.; Kornfeldt, A., A Quartz Crystal Microbalance Study of the Adsorption of Asphaltenes and Resins onto a Hydrophilic Surface. *Journal of Colloid and Interface Science* 2002, *247*, (2), 342-350.
49. Dai, C.; Zhao, J.; Giammar, D. E.; Pasteris, J. D.; Zuo, X.; Hu, Y., Heterogeneous Lead Phosphate Nucleation at Organic–Water Interfaces: Implications for Lead Immobilization. *ACS Earth and Space Chemistry* 2018, *2*, (9), 869-877.
50. Dai, C.; Hu, Y., Fe (III) hydroxide nucleation and growth on quartz in the presence of Cu (II), Pb (II), and Cr (III): metal hydrolysis and adsorption. *Environmental science & technology* 2014, *49*, (1), 292-300.
51. Dai, C.; Zuo, X.; Cao, B.; Hu, Y., Homogeneous and Heterogeneous (Fe_x, Cr_{1-x})$(OH)_3$ Precipitation: Implications for Cr Sequestration. *Environmental Science & Technology* 2016, *50*, (4), 1741-1749.
52. Dai, C.; Stack, A. G.; Koishi, A.; Fernandez-Martinez, A.; Lee, S. S.; Hu, Y., Heterogeneous nucleation and growth of barium sulfate at organic–water interfaces: interplay between surface hydrophobicity and Ba^{2+} adsorption. *Langmuir* 2016, *32*, (21), 5277-5284.
53. Dai, C.; Lin, M.; Hu, Y., Heterogeneous Ni-and Cd-Bearing Ferrihydrite Precipitation and Recrystallization on Quartz under Acidic pH Condition. *ACS Earth and Space Chemistry* 2017, *1*, (10), 621-628.
54. Frisch, M. J.; Trucks, G.; Schlegel, H. B.; Scuseria, G.; Robb, M.; Cheeseman, J.; Scalmani, G.; Barone, V.; Mennucci, B.; Petersson, G., Gaussian 09, revision A. 1. *Gaussian Inc. Wallingford CT* 2009, *27*, 34.
55. Nangia, S.; Garrison, B. J. In *Study of silica-water interactions on mineral surfaces*, 2007; American Chemical Society: 2007; pp PHYS-221.
56. Hadjiivanov, K., Chapter Two - Identification and Characterization of Surface Hydroxyl Groups by Infrared Spectroscopy. In *Advances in Catalysis*, Jentoft, F. C., Ed. Academic Press: 2014; Vol. 57, pp 99-318.
57. *BIOVA Materials Studio 2016*, Dassault Systèmes BIOVIA: San Diego, CA, 2016.
58. Lee, C.; Yang, W.; Parr, R. G., Development of the Colle-Salvetti correlation-energy formula into a functional of the electron density. *Physical Review B* 1988, *37*, (2), 785-789.
59. Becke, A. D., A new mixing of Hartree–Fock and local density-functional theories. *The Journal of Chemical Physics* 1993, *98*, (2), 1372-1377.
60. McLean, A. D.; Chandler, G. S., Contracted Gaussian basis sets for molecular calculations. I. Second row atoms, Z=11–18. *The Journal of Chemical Physics* 1980, *72*, (10), 5639-5648.
61. Raghavachari, K.; Trucks, G. W., Highly correlated systems. Excitation energies of first row transition metals Sc–Cu. *The Journal of Chemical Physics* 1989, *91*, (2), 1062-1065.
62. Reed, A. E.; Weinstock, R. B.; Weinhold, F., Natural population analysis. *The Journal of Chemical Physics* 1985, *83*, (2), 735-746.
63. James, R. O.; Healy, T. W., Adsorption of hydrolyzable metal ions at the oxide—water interface. III. A thermodynamic model of adsorption. *Journal of Colloid and Interface Science* 1972, *40*, (1), 65-81.
64. Liu, C.; Min, F.; Liu, L.; Chen, J.; Du, J., Mechanism of hydrolyzable metal ions effect on the zeta potential of fine quartz particles. *Journal of Dispersion Science and Technology* 2018, *39*, (2), 298-304.

65. Lamb, A. C. M.; Grieser, F.; Healy, T. W., The adsorption of uranium (VI) onto colloidal TiO2, SiO2 and carbon black. *Colloids and Surfaces A: Physicochemical and Engineering Aspects* 2016, *499*, 156-162.
66. Zhang, Z.; Fenter, P.; Kelly, S. D.; Catalano, J. G.; Bandura, A. V.; Kubicki, J. D.; Sofo, J. O.; Wesolowski, D. J.; Machesky, M. L.; Sturchio, N. C.; Bedzyk, M. J., Structure of hydrated Zn2+ at the rutile TiO2 (110)-aqueous solution interface: Comparison of X-ray standing wave, X-ray absorption spectroscopy, and density functional theory results. *Geochimica et Cosmochimica Acta* 2006, *70*, (16), 4039-4056.
67. James, R. O.; Healy, T. W., Adsorption of hydrolyzable metal ions at the oxide—water interface. III. A thermodynamic model of adsorption. *J. Colloid Interface Sci.* 1972, *40*, (1), 65-81.
68. Cao, X.; Ma, L. Q.; Rhue, R. D.; Appel, C., Mechanisms of Lead, Copper, and Zinc Retention by Phosphate Rock. *Environmental Pollution* 2004, *131*, 435-444.
69. Sabur, M. A.; Goldberg, S.; Gale, A.; Kabengi, N.; Al-Abadleh, H. A., Temperature-Dependent Infrared and Calorimetric Studies on Arsenicals Adsorption from Solution to Hematite Nanoparticles. *Langmuir* 2015, *31*, (9), 2749-2760.
70. Kabengi, N. J.; Daroub, S. H.; Rhue, R. D., Energetics of Arsenate Sorption on Amorphous Aluminum Hydroxides Studied Using Flow Adsorption Calorimetry. *Journal of Colloid and Interface Science* 2006, *297*, (1), 86-94.
71. Bellucci, F.; Lee, S. S.; Kubicki, J. D.; Bandura, A.; Zhang, Z.; Wesolowski, D. J.; Fenter, P., Rb+ Adsorption at the Quartz(101)–Aqueous Interface: Comparison of Resonant Anomalous X-ray Reflectivity with ab Initio Calculations. *The Journal of Physical Chemistry C* 2015, *119*, (9), 4778-4788.
72. Lee, S. S.; Fenter, P.; Nagy, K. L.; Sturchio, N. C., Real-time observation of cation exchange kinetics and dynamics at the muscovite-water interface. *Nature Communications* 2017, *8*, 15826.
73. Kroutil, O.; Chval, Z.; Skelton, A. A.; Předota, M., Computer Simulations of Quartz (101)–Water Interface over a Range of pH Values. *The Journal of Physical Chemistry C* 2015, *119*, (17), 9274-9286.
74. Pfeiffer-Laplaud, M.; Gaigeot, M.-P., Adsorption of Singly Charged Ions at the Hydroxylated (0001) α-Quartz/Water Interface. *The Journal of Physical Chemistry C* 2016, *120*, (9), 4866-4880.
75. Prelot, B.; Lantenois, S.; Charbonnel, M.-C.; Marchandeau, F.; Douillard, J. M.; Zajac, J., What are the Main Contributions to the Total Enthalpy of Displacement Accompanying the Adsorption of Some Multivalent Metals at the Silica–Electrolyte Interface? *Journal of Colloid and Interface Science* 2013, *396*, 205-209.
76. Luo, Y. R., *Comprehensive Handbook of Chemical Bond Energies*. CRC Press: Boca Raton, Fl, 2007.
77. Smith, D. W., Ionic hydration enthalpies. *Journal of Chemical Education* 1977, *54*, (9), 540.
78. Bunker, B. C.; Casey, W. H., Solvated Ions in Water. In *The Aqueous Chemistry of Oxides*, Oxford University Press: New York City, 2016.
79. Ball, J. W.; Nordstrom, D. K., Critical Evaluation and Selection of Standard State Thermodynamic Properties for Chromium Metal and Its Aqueous Ions, Hydrolysis Species, Oxides, and Hydroxides. *Journal of Chemical & Engineering Data* 1998, *43*, (6), 895-918.

For TOC only

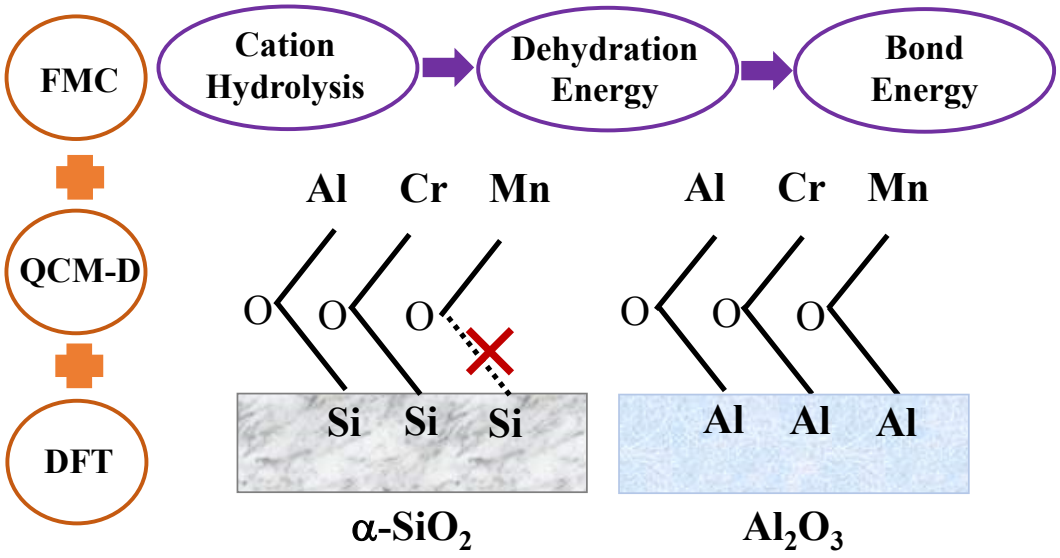
FMC
QCM-D
DFT
Cation Hydrolysis
Dehydration Energy
Bond Energy
Al Cr Mn
O O O
Si Si Si
α-SiO2
Al Cr Mn
O O O
Al Al Al
Al2O3